Acta Mechanica Solida Sinica
https://doi.org/10.1007/s10338-019-00139-x
ISSN 1860-2134

Scattering Analysis and Optimization of Spherical Acoustic Cloak with Unideal Pentamode Material

Xin Nie[1] **Yi Chen**[1] **Xiaoning Liu**[1*]

([1] *Key Laboratory of Dynamics and Control of Flight Vehicle, Ministry of Education, School of Aerospace Engineering, Beijing Institute of Technology, Beijing 100081, China*)

Received 13 February 2019; revision received 29 August 2019; Accepted 2 September 2019

ABSTRACT The acoustic scattering is theoretically studied in this paper for three-dimensional spherical cloak composed of unideal pentamode material, for which small shear rigidity is always inevitable for a real designed microstructure. A theoretical formulation is developed to efficiently evaluate the cloaking performance. The generic scattering feature of the cloak and the effects of material imperfectness and inner cloak boundary constraints are systematically examined. The preferable constraint type and the critical imperfectness parameter of the material are identified for possible broadband invisibility. In addition, a very practical lining shell scheme is proposed to tune the constraint strength on the inner boundary. By combining the theoretical model with optimization algorithm, it is further proved that the cloak can be reduced by several piecewise-uniform layers and optimized to achieve excellent invisibility in targeted frequency bands. The study will provide valuable guidance for the future microstructural design of cloaks.

KEY WORDS Pentamode material, Spherical acoustic cloak, Scattering calculation, Boundary effect, Optimization

1. Introduction

Since the advent of transformation method for electromagnetic (EM) wave and the metamaterial technique [1–3], the envisioning cloaks and other devices aiming to freely manipulate the physical field have been a continuously fascinating subject for the past years [4, 5]. For acoustic waves, the cloak was firstly proposed by recognizing the analogy between the Helmholtz equation and the EM one [6, 7]; the cloak material needs to be kind of acoustic fluids with anisotropic density. A variety of meta-fluids realizing anisotropic density have been suggested [8–10]. However, current meta-fluid schemes suffer from either narrow frequency band, or quite limited achievable density anisotropy. The two principal densities usually differ by five times for air sound [10], and only differ by two times for water sound [11]. Therefore, only the carpet cloak [12] has been experimentally demonstrated so far because much larger anisotropy is required for omnidirectional cloaks.

Besides the mentioned meta-fluids, there is, however, an alternative route for the acoustic cloak making use of the solid-based pentamode material (PM). PM was originally defined by Milton and Chaecheve in answering the question of whether an arbitrarily given positive definite symmetric elastic tensor corresponds to a material realization [13]. PM is the degenerated solid material which has only one nonzero eigenvalue among the six eigenvalues of its elastic tensor. Accordingly, like the acoustic

* Corresponding author. E-mail:liuxn@bit.edu.cn

Published online: 21 September 2019

fluid, PM can only sustain a single stress state, which is not necessarily the hydrostatic stress. Thus, the material can also be regarded as a generalized fluid with anisotropy. In this sense, PM might be responsible for the controlling of acoustic wave. Norris proposed that the transformed acoustic equation has the same form as the wave equation of PM [14]. Through careful microstructural design to tune the shear rigidity, PM can be approximated by solid materials. The greatest advantage of PM is that unlike many other metamaterials, they are not resonance-based, and are theoretically with broadband. Other advantages include sharper control benefitting from higher anisotropy and the solid nature of devices. These merits stimulated intense research on PM, e.g. the PM transformation theory [15, 16], acoustic wave controlling applications [17–22], and PM microstructure design [23–26]. A PM acoustic cloak in cylindrical configuration with gradient microstructure was designed recently, and its manipulation capability for underwater sound was experimentally verified [27, 28].

A specific issue pertaining to PM cloaks is that the practical solid-based PM cannot be ideal (i.e. with zero shear resistance) in order to be stable. A real PM in fact falls into the category of orthotropic solids. For the several fabricated examples, the ratios of shear modulus to bulk modulus are usually about 1% for two-dimensional (2D) PM and 1‰ for three-dimensional (3D) PM, but not zero [25, 27]. The small shear rigidity of unideal PM induces extra shear modes in addition to the pseudo-pressure mode in ideal PM [27]. It has been numerically shown for cylindrical PM cloak that unideal PM causes shear resonance in cloak shell and peaks in scattering spectrum, thus the broadband effectivity will be damaged to a certain extent. On the other hand, the constraint condition on the inner boundary of the cloak can significantly influence the concealing effect since wave can penetrate the cloak due to the imperfection. Unideal PM renders the choice of inner boundary condition subtler since the cloak shell is actually solid. In previous studies of ideal PM cloak [15, 29, 30], the radially fixed inner surface boundary is assumed to demonstrate the best invisibility. However, such a boundary constraint cannot be easily applied to a real PM cloak, especially for water sound applications. As for elastic wave in the PM cloak, ordinary solids easily couple with the PM and can hardly restrict the motion of the inner surface. From a practical point of view, the easiest implementation is a free inner surface. As will be shown, however, the free inner surface severely destroys the cloaking performance. Due to the much complex wave propagation in gradient unideal PM, most analytical contributions consider the PM as ideal ones with zero shear rigidity [17, 30], and very limited attention has been paid to the impact of imperfectness of PM as well as the boundary effect on the acoustic cloak.

In this work, we develop an analytical state space formulation to analyse the scattering of unideal PM cloak immersed in fluids under acoustic illumination. Based on the method, the effects of material parameters and inner boundary conditions on the cloaking performance are systematically investigated. We also propose a lining shell scheme to tune the constraint strength on the inner boundary, and it turns out that there is optimized strength in an average sense. Further, upon the effectivity of the scattering analysis, we are able to explore the optimization of cloak with a few piecewise layers in order to achieve good concealing over a targeted frequency range. The paper is organized in five parts including this introduction. In Sect. 2, the model of spherical acoustic cloak with unideal PM is defined and the scattering analysis is developed. In Sect. 3, numerical examples are presented in order to explain the generic scattering feature of the cloak and the influences of inner boundary and PM imperfectness. Section 4 is concerned with the optimization of the parameters of layered cloak with unideal PM. Finally, concluding remarks are given in Sect. 5.

2. Model of Spherical Acoustic Cloak with Imperfect PM

PM is characterized by an elastic tensor with a single nonzero eigenvalue; hence, the elastic tensor can be expressed as [13, 14]

$$\boldsymbol{C} = K\boldsymbol{S} \otimes \boldsymbol{S} \tag{1}$$

where $\boldsymbol{S}$ is a non-dimensional symmetric characteristic tensor of rank two, and K has the dimension of a fluid bulk modulus. The material thus can only withstand one stress state proportional to the characteristic tensor, $\boldsymbol{\sigma} = p\boldsymbol{S}$, with p being termed as pseudo-pressure [14]. In other words, for a general strain $\boldsymbol{\varepsilon}$, only the part projected onto $\boldsymbol{S}$ matters in the constitutive relation

$$p = K\left(\boldsymbol{S} : \boldsymbol{\varepsilon}\right) = K\left(\boldsymbol{S} : \nabla \boldsymbol{u}\right) \tag{2}$$

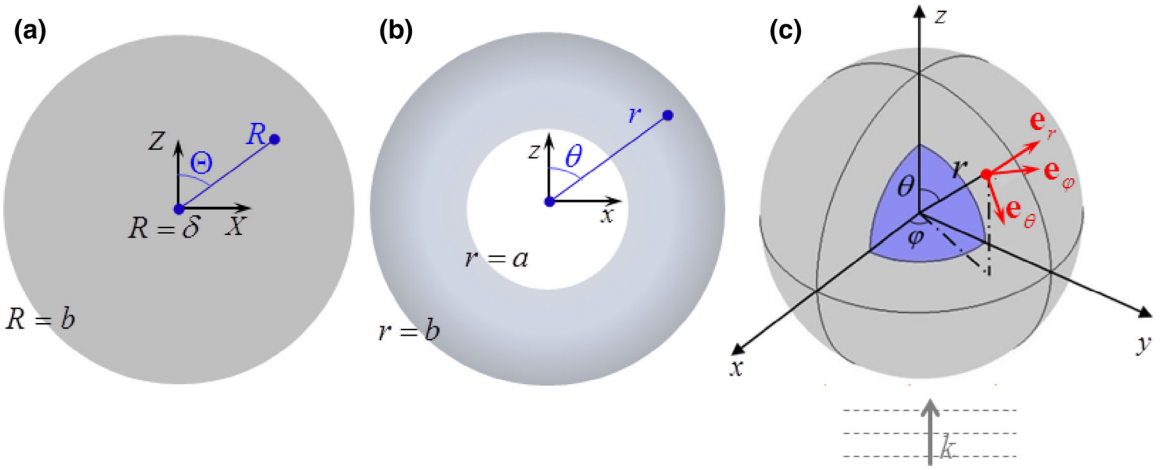

Fig. 1. Transformation approach of spherical cloak: **a** XZ section of virtual space; **b** xz section of physical space; **c** oblique view and coordinate frame, with k the incidental wave vector

and the remaining five zero-energy deformation modes orthogonal to $\boldsymbol{S}$ belong to zero-energy (easy) modes, hence the name *pentamode*. Taking the equilibrium equation into account, the PM wave equation expressed in pseudo-pressure p can be obtained as

$$\frac{\partial^2 p}{\partial t^2} = K\boldsymbol{S} : \nabla\left(\rho^{-1}\boldsymbol{S}\nabla p\right) \tag{3}$$

where ρ is the density. An additional requirement is that the tensor $\boldsymbol{S}$ of the PM has to be divergence-free in order for the material to be at static equilibrium under uniform pseudo-pressure [14]. For the trivial isotropic case of $\boldsymbol{S} = \boldsymbol{I}$, Eq. (3) reduces to the traditional acoustic wave equation. As for the pentamode transformation acoustics, it has been proved that under a curvilinear coordinate mapping $\boldsymbol{x} = \boldsymbol{x}(\boldsymbol{X})$, the wave equation in traditional fluid with bulk modulus K_0 and density ρ_0 is,

$$\frac{\partial^2 p}{\partial t^2} = K_0\nabla\left(\rho_0^{-1}\nabla p\right) \tag{4}$$

which could be transformed into the same form as that of a PM, Eq. (3), provided any divergence-free $\boldsymbol{S}$ field. The material properties of the PM are bridged to those of virtual space by the transformation geometry as,

$$\boldsymbol{\rho}^{-1} = \rho_0^{-1}J^{-1}\boldsymbol{S}^{-1}\boldsymbol{F}\boldsymbol{F}^{\mathrm{T}}\boldsymbol{S}^{-1}, \quad \boldsymbol{C} = K_0 J\boldsymbol{S}\otimes\boldsymbol{S} \tag{5}$$

where $\boldsymbol{F} = \partial\boldsymbol{x}/\partial\boldsymbol{X}$ is the deformation gradient, and $J = \det\boldsymbol{F}$. It should be noted from Eq. (5) that the density is generalized to a tensor, which makes the functional PM realization deduced from arbitrary transformation still an open question. However, for the irrotational transformation (i.e. $\boldsymbol{F}$ is symmetric), we can choose $\boldsymbol{S} = J^{-1}\boldsymbol{F}$, which is naturally divergence-free, and the resulting PM has isotropic density:

$$\boldsymbol{\rho} = \rho\boldsymbol{I},\ C = K\boldsymbol{S}\otimes\boldsymbol{S},\ \rho = J^{-1}\rho_0,\ K = JK_0 \tag{6}$$

The spherical cloak considered in this paper falls in this case. As shown in Fig. 1, a radial symmetric mapping in spherical coordinates, $R = R(r)$, $\Theta = \theta$, $\Phi = \phi$, is assumed, and the deformation gradient is then $\boldsymbol{F} = \mathrm{diag}\,[1/R',\ r/R,\ r/R]$ in the spherical coordinate system, where $R' = \mathrm{d}R(r)/\mathrm{d}r$. By using Eq. (6), the continuously varying elastic matrix in Voigt form and the density of a spherical cloak with ideal PM can be explicitly given as

$$\rho = \rho \boldsymbol{I}, \boldsymbol{C} = \begin{pmatrix} K_r & \sqrt{K_r K_\perp} & \sqrt{K_r K_\perp} & 0 & 0 & 0 \\ & K_\perp & K_\perp & 0 & 0 & 0 \\ & & K_\perp & 0 & 0 & 0 \\ & & & 0 & 0 & 0 \\ & \text{sym} & & & 0 & 0 \\ & & & & & 0 \end{pmatrix}$$
$$\rho = \rho_0 \frac{R^2 R'}{r^2}, K_r = K_0 \frac{R^2}{r^2 R'}, K_\perp = K_0 R' \tag{7}$$

where the symbol $\perp$ stands for the θ or ϕ direction perpendicular to the radial one. Any choice of continuous mapping function $R(r)$ satisfying $R(b) = b$ and $R(a) = \delta$ can be taken, where a and b are, respectively, the inner and outer radii of the cloak shell (Fig. 1b), and a small radius in the virtual space $\delta \ll a$ is introduced to avoid the material singularity. From the viewpoint of microstructure realization, since a PM cloaking shell with constant density is easier to design [27], a mapping function producing constant density is adopted here [15]:

$$R(r) = \sqrt[3]{b^3 + \frac{b^3 - \delta^3}{b^3 - a^3}(r^3 - b^3)} \tag{8}$$

There are several facts preventing a real cloak from being perfectly invisible over broadband frequency. Such reasons can be that the cloak is not mapped out from an infinitesimal point in the virtual space (i.e. $\delta \neq 0$), the smoothly gradient cloak material cannot be attained due to the finite size of microstructure, etc. For a PM cloak, the man-made PM is always unideal and cannot be strictly of the form of Eq. (7), leading to an additional imperfection. In Eq. (7), the zero shear modulus and the dependence of off-diagonal items on the diagonal ones ensure the single nonzero eigenvalue of the elastic matrix. However, for the real PM machined from solid materials, one can only expect the shear resistance as small as possible, and the approximating PM is in fact the transversely isotropic solid material with the symmetrical axis in the r-direction,

$$\boldsymbol{C} = \begin{pmatrix} K_r & K_{r\perp} & K_{r\perp} & 0 & 0 & 0 \\ & K_\perp & K_\perp - 2G_{\perp\perp} & 0 & 0 & 0 \\ & & K_\perp & 0 & 0 & 0 \\ & & & G_{r\perp} & 0 & 0 \\ & \text{sym} & & & G_{r\perp} & 0 \\ & & & & & G_{\perp\perp} \end{pmatrix} \tag{9}$$

To characterize the degree of imperfectness of the PM, three non-dimensional parameters are defined as

$$\xi = \frac{K_{r\perp}}{\sqrt{K_r K_\perp}}, \quad \zeta = \frac{G_{r\perp}}{\sqrt{K_r K_\perp}}, \quad \eta = \frac{G_{\perp\perp}}{\sqrt{K_r K_\perp}} \tag{10}$$

In order to approach an ideal PM, $|\xi - 1| \ll 1$, $\zeta \ll 1$ and $\eta \ll 1$ should be guaranteed. For the isotropic case, requiring one of the inequalities is sufficient. For anisotropic materials, all of the imperfectness parameters should be restricted in the microstructural design, and it turns out that the magnitudes of each one may have different effects on the cloaking performance.

Next, we analyse the acoustic scattering of an immersed spherical cloak with imperfect PM, i.e. essentially a shell of transversely isotropic solid of gradient density $\rho(r)$ and modulus $\boldsymbol{C}(r)$ with the material principal axis aligning with the spherical frame (Eq. (9)). Since it is not possible to give a closed-form solution for such a problem, a semi-analytical state space approach traditionally used for laminated orthotropic layers [31, 32] is adopted here.

Consider a plane wave with circular frequency ω incidents from the bottom along the $+z$ direction, $p_{\text{in}} = \exp(\mathrm{i}k_0 z)$, where time dependence $\exp(-\mathrm{i}\omega t)$ is adopted. The incident plane wave can be decomposed into spherical harmonics

$$P_{\text{in}} = \sum_{n=0}^{\infty} a_n j_n(k_0 r) P_n(\cos\theta) \tag{11}$$

where j_n and P_n are the spherical Bessel function and Legendre function of the nth order, respectively, $a_n = \mathrm{i}^n(2n+1)$, and $k_0 = \omega/c_0$ is the wave number with $c_0 = (K_0/\rho_0)^{1/2}$ being wave speed of the background fluid. Similarly, the scattered pressure in background fluid can be expressed as

$$P_{\mathrm{sc}} = \sum_{n=0}^{\infty} b_n h_n^{(1)}(k_0 r) P_n(\cos\theta) \tag{12}$$

where b_n is the nth scattering coefficient to be determined, and $h_n^{(1)}$ is the nth-order spherical Hankel function of the first kind. To work out the scattering coefficient, the wave transmission in each PM layer needs to be considered and joined at layer interfaces and the cloak's inner boundary. Considering the model symmetry, mode orthogonality of different orders and the continuity requirement at the PM/fluid interface, the ansatz

$$u_r = \sum_{n=0}^{\infty} u_{nr}(r) P_n(\cos\theta), \quad u_\theta = \sum_{n=0}^{\infty} u_{n\theta}(r) P_n'(\cos\theta), \quad u_\varphi = 0 \tag{13}$$

for displacements and

$$\begin{aligned} \sigma_r &= \sum_{n=0}^{\infty} \sigma_{nr}(r) P_n(\cos\theta), \qquad \sigma_\theta = \sum_{n=0}^{\infty} \sigma_{1n\theta}(r) P_n(\cos\theta) + \sigma_{2n\theta}(r)(\cot\theta) P_n'(\cos\theta) \\ \sigma_{r\theta} &= \sum_{n=0}^{\infty} \sigma_{nr\theta}(r) P_n'(\cos\theta), \quad \sigma_\varphi = \sum_{n=0}^{\infty} \sigma_{1n\varphi}(r) P_n(\cos\theta) + \sigma_{2n\varphi}(r) P_n''(\cos\theta) \\ \sigma_{r\varphi} &= \sigma_{\theta\varphi} = 0 \end{aligned} \tag{14}$$

for stresses are adopted, where a prime in superscript means the derivative. Considering the decomposition Eqs. (13) and (14) in conjunction with the constitutive equation and momentum equation in spherical coordinates for the transversely isotropic cloak shell (detailed in "Appendix"), for each scattering order, a group of ordinary differential equations with respect only to r can be obtained. In particular, by defining the state vector $\boldsymbol{D}_n(r) = [u_{nr},\ u_{n\theta},\ \sigma_{nr},\ \sigma_{nr\theta}]^{\mathrm{T}}$ for order n, we obtain

$$\frac{\mathrm{d}\boldsymbol{D}_n(r)}{\mathrm{d}r} = \boldsymbol{P}_n(r)\boldsymbol{D}_n(r) \tag{15}$$

where

$$\boldsymbol{P}_n(r) = \begin{pmatrix} \frac{-2B}{r} & \frac{n(n+1)B}{r} & \frac{1}{K_r} & 0 \\ -\frac{1}{r} & \frac{1}{r} & 0 & \frac{1}{G_{r\theta}} \\ \frac{-4A}{r^2} - \rho\omega^2 & \frac{2n(n+1)A}{r^2} & \frac{2(B-1)}{r} & \frac{n(n+1)}{r} \\ \frac{2A}{r^2} & \frac{-2G_{\theta\varphi} - n(n+1)(BK_{r\theta} - K_\theta)}{r^2} - \rho\omega^2 & -\frac{B}{r} & -\frac{3}{r} \end{pmatrix} \tag{16}$$

and $A = (G_{\theta\varphi}K_r + K_{r\theta}^2 - K_r K_\theta)/K_r$, $B = K_{r\theta}/K_r$. Equation (15) is difficult to be analytically solved since $\boldsymbol{P}_n$ is a function of r. To proceed, the cloak shell is evenly divided into N piecewise-uniform concentric layers labelled by $1 \sim N$ from the inner most, with each layer being characterized by five (transversely isotropic) elastic constants and densities, i.e. for the jth layer bounded by $r_{j-1} < r < r_j$, $\rho_j = \rho((r_{j-1} + r_j)/2)$, $\boldsymbol{C}_j = \boldsymbol{C}((r_{j-1} + r_j)/2)$. The background domain outside the cloak is filled with homogeneous fluid (ρ_0, K_0), and is defined as layer $(N+1)$. If N is sufficiently large, $\boldsymbol{P}_n(r)$ in each very thin layer j can be reasonably treated as a constant matrix, and denoted as $\boldsymbol{P}_{jn} = \boldsymbol{P}_n\left((r_{j-1} + r_j)/2\right)$, then Eq. (15) admits an exponential solution and the state vectors at the two edges of layer j are related to

$$\boldsymbol{D}_n(r_j) = \exp\left[(r_j - r_{j-1})\,\boldsymbol{P}_{jn}\right]\boldsymbol{D}_n(r_{j-1}) \tag{17}$$

Because of continuity of the state vectors, the state vector $\boldsymbol{D}_n(r_N)$ and $\boldsymbol{D}_n(r_0)$at the outer most and inner most surfaces of the cloak, respectively, are related to

$$\boldsymbol{D}_n(r_N) = \boldsymbol{T}_n\boldsymbol{D}_n(r_0), \quad \boldsymbol{T}_n = \prod_{j=1}^{N} \exp\left[(r_j - r_{j-1})\,\boldsymbol{P}_{jn}\right] \tag{18}$$

Finally, the state variables of $\boldsymbol{D}_n(r_N)$have to match the background acoustic wave at the fluid–PM interface:

$$\begin{aligned} u_{nr}(r_N) &= \frac{1}{\rho_0\omega^2}\left(a_n j_n'(k_0 r_N) + b_n h_n'^{(1)}(k_0 r_N)\right) \\ \sigma_{nr}(r_N) &= -\left(a_n j_n(k_0 r_N) + b_n h_n^{(1)}(k_0 r_N)\right), \quad \sigma_{nr\theta}(r_N) = 0 \end{aligned} \tag{19}$$

At the cloak's inner surface, various boundary conditions can be assumed and we will see that the boundary will significantly affect the cloak behaviour. Typically, we have $u_{nr}(r_0) = u_{n\theta}(r_0) = 0$ for fixed, $\sigma_{nr}(r_0) = \sigma_{nr\theta}(r_0) = 0$ for free, and$u_{nr}(r_0) = \sigma_{nr\theta}(r_0) = 0$ for radially fixed inner boundaries, respectively. With some algebraic manipulation, the scattering coefficient of each order can be solved for fixed, free and radially fixed inner boundaries as

$$b_n = -a_n \frac{(T_{n33}T_{n42} - T_{n32}T_{n43})j_n'(k_0 r_N) - (T_{n12}T_{n43} - T_{n13}T_{n42})K_0 k_0^2 j_n(k_0 r_N)}{(T_{n33}T_{n42} - T_{n32}T_{n43})h_n'^{(1)}(k_0 r_N) - (T_{n12}T_{n43} - T_{n13}T_{n42})K_0 k_0^2 h_n^{(1)}(k_0 r_N)} \tag{20a}$$

$$b_n = -a_n \frac{(T_{n32}T_{n41} - T_{n31}T_{n42})j_n'(k_0 r_N) - (T_{n11}T_{n42} - T_{n12}T_{n41})K_0 k_0^2 j_n(k_0 r_N)}{(T_{n32}T_{n41} - T_{n31}T_{n42})h_n'^{(1)}(k_0 r_N) - (T_{n11}T_{n42} - T_{n12}T_{n41})K_0 k_0^2 h_n^{(1)}(k_0 r_N)} \tag{20b}$$

$$b_n = -a_n \frac{(T_{n33}T_{n44} - T_{n34}T_{n43})j_n'(k_0 r_N) - (T_{n14}T_{n43} - T_{n13}T_{n44})K_0 k_0^2 j_n(k_0 r_N)}{(T_{n33}T_{n44} - T_{n34}T_{n43})h_n'^{(1)}(k_0 r_N) - (T_{n14}T_{n43} - T_{n13}T_{n44})K_0 k_0^2 h_n^{(1)}(k_0 r_N)} \tag{20c}$$

respectively, where T_{nij} is the components of the transmittance matrix $\boldsymbol{T}_n$.

In the following, we adopt the total scattering cross section (TSCS) which assesses the total scattering in all directions to quantify the cloaking performance. The TSCS is defined as the ratio between the scattered and the incident energies onto the cloak. With the help of determined scattering coefficients, the TSCS in this scenario can be written as

$$\mathrm{TSCS} = \frac{2}{k_0^2 r_0^2}\sum_{n=0}^{\infty}\frac{2}{2n+1}|b_n|^2 \tag{21}$$

With the asymptotic expansion of spherical Hankel function, the far-field scattered pressure of Eq. (12) can be approximated as

$$p_{\mathrm{sc}} \approx \frac{1}{r}A(\theta)\exp(\mathrm{i}k_0 r), A(\theta) = \sum_{n=0}^{\infty} b_n \frac{1}{k_0}\exp\left[-\mathrm{i}\left(\frac{n\pi}{2} + \frac{\pi}{2}\right)\right]P_n(\cos\theta) \tag{22}$$

where $A(\theta)$ is the form function of the scattered pressure and parameter θ is the azimuth angle. $A(0)$ and $A(\pi)$ stand for the forward and backward scattering coefficients, respectively.

3. Numerical Result for Cloak with Continuously Varying Parameters

3.1. Generic Scattering Spectrum

We first consider a spherical PM cloak defined from the above transformation method. The inner and outer radii of the cloak shell are set as a and $b = 2a$, respectively, and the virtual space small parameter is $\delta = a/5$. Using the mapping function of Eq. (8), the cloak's major material properties ρ, K_r and $K_\perp$ are determined from Eq. (7). To consider the imperfectness, $\xi = 0.99, \zeta = \eta = 0.01$ are introduced to bring the tiny shear resistance into the material, and this renders the cloak material to be transversely isotropic solid defined by Eqs. (8)–(10). Other choices of δ and the mapping function will not affect the main conclusion. The displacements on the inner surface of the cloak shell are assumed to be fixed. The influences of other boundary constraints as well as the degree of imperfectness will be examined in the following subsections.

Figure 2a displays the theoretically calculated TSCS spectrum in the black curve over $ka/\pi = 0 \sim 1.2$. In the theoretical model, up to 21 orders of spherical harmonics are used for truncation and the cloak shell is evenly discretized into 1200 layers to ensure sufficient approximation of the continuous cloak and convergence. For verification, the TSCS spectrum is also swept for the same cloak configuration by using the finite element software COMSOL Multiphysics, shown in the figure by red dots. It is shown in Fig. 2a that the theoretical TSCS spectrum matches the FEM simulation very well, which validates the effectivity and accuracy of the developed method. Since the FEM simulation

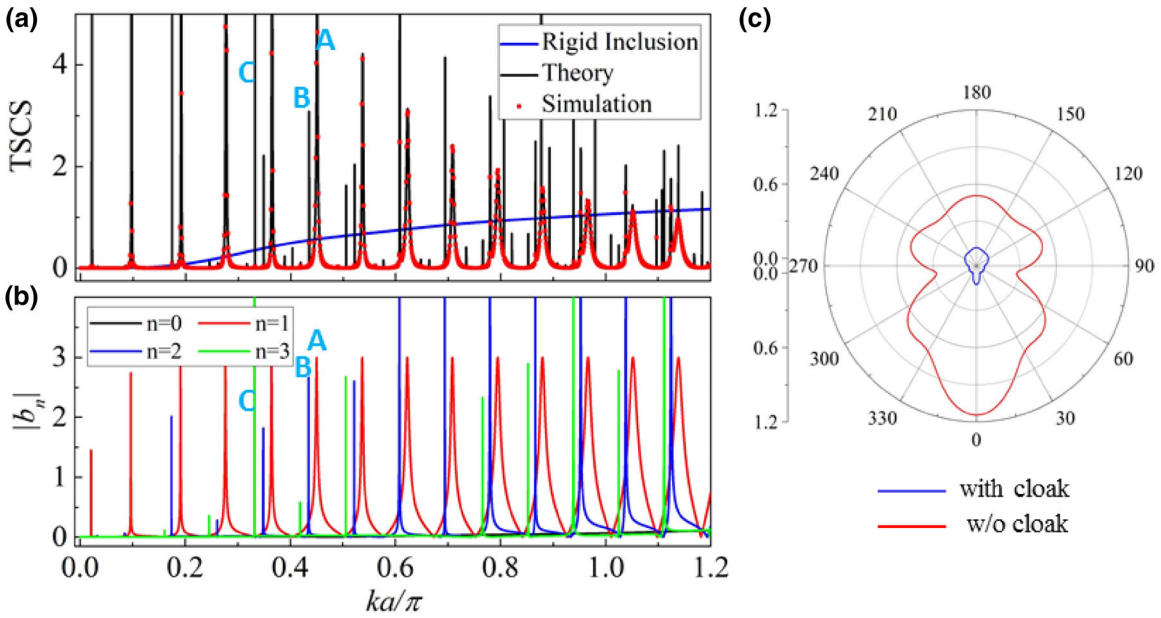

Fig. 2. **a** Total scattering cross section for a rigid sphere and PM cloak with fixed inner boundary; **b** scattering coefficient amplitudes of the first four orders; **c** far-field scattering pressure amplitude at $ka = 1.1\,\pi$. (Color figure online)

is quite time-consuming and even overwhelming at higher frequencies, the sweeping resolution of the spectrum (1000 points per ka/π) cannot be as fine as that in the analytical formulation (10000 points per ka/π), hence some very narrow peaks are not checked out by the numerical method. However, the exact matching on the shown part of curves and peaks sufficiently validates the developed analytical model. In comparison with the case of a rigid sphere of radius a without cloak (the blue curve), the PM cloak significantly lowers scattering for most frequencies; however, the TSCS spectrum contains regularly placed sharp peaks which obviously relate to some resonances.

Besides the efficiency, the proposed method can give more insights into the mechanism of the scattering spectrum by isolating the scattering coefficient of each order, as shown in Fig. 2b, where $|b_0| \sim |b_3|$ are plotted. Figure 2 shows that there is one-to-one correspondence for each peak in the TSCS spectrum and a certain order of scattering coefficient. It is remarkable that no resonance peaks are observed for the zeroth-order scattering $|b_0|$, which suggests that the peaks are due to the shear wave in unideal PM since the zeroth-order mode is breathe-like and does not interplay with the shear mode. In practice, since there always exists material or environmental damping in a real system, the very sharp peaks are hopefully erased, thus for the fixed inner boundary, the harmful wide peaks are mainly contributed by the first-order scattering (the red curves in Fig. 2b). Figure 2c gives the polar plot of the far-field scattering radiation at $ka = 1.1\pi$ where no peak is there. It is seen that the far-field pressure is reduced by the cloak compared to the bare rigid sphere.

To further confirm the shear-related origin of the peak forest in the scattering spectrum, it is reasonable to check out the curl field of the displacement in cloak material. Since $u_\varphi = 0$ and u_r and u_θ are independent of φ, the curl is taken in axisymmetric section by $(\text{curl}\ \boldsymbol{u})_\varphi = \partial_\theta u_r - \partial_r u_\theta$. Figure 3 shows $(\text{curl}\ \boldsymbol{u})_\varphi$ and its phase $\arg[(\text{curl}\ \boldsymbol{u})_\varphi]$ at three selected frequencies lying on peaks as highlighted by A∼C in Fig. 2. A case without peak at frequency $ka = 0.50\pi$ is also added for comparison. Note that peaks A, B and C come, respectively, from the 1st-, 2nd- and 3rd-order scattering. It is observed that at the TSCS peaks, the displacement curl is much pronounced, and the phase shows a standing wave pattern matching exactly the scattering order. For odd-order resonances (peaks A and C), the phase field is dominated by $\pm\pi$ and 0, while for even-order resonance (peak B), the phase pattern is dominated by $\pm\pi/2$, and these clearly implies the presence of shear standing waves. It is remarkable that the resonant scattering peaks found here are essentially different from those caused by whispering-gallery waves, which are also present for isotropic elastic spherical scatter immersed

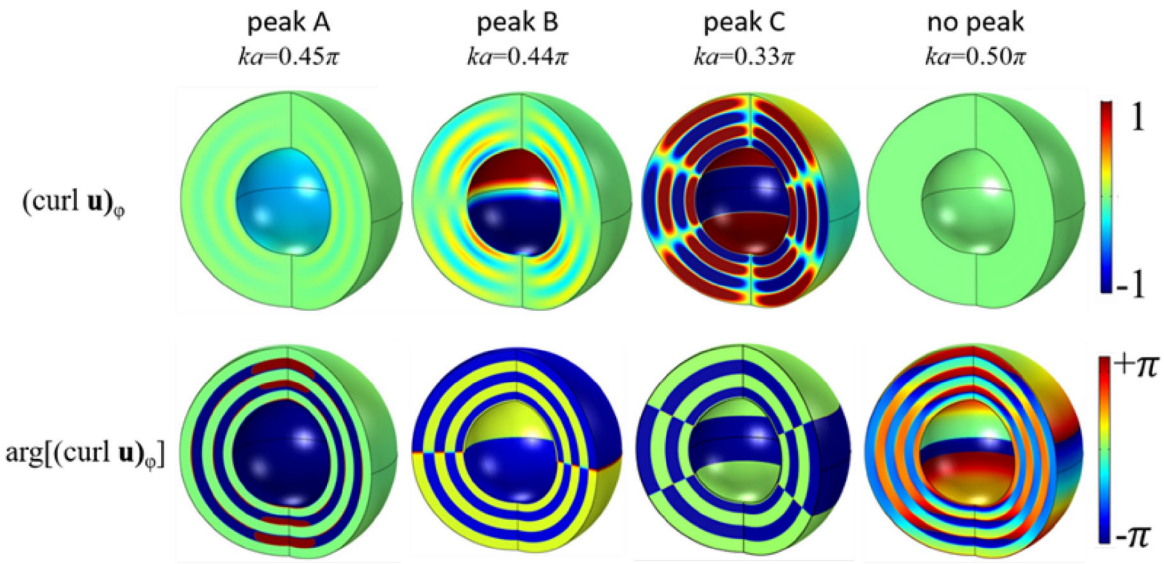

Fig. 3. Displacement curl and the corresponding phase fields in the cloak shell

in fluids [33, 34]. The whispering-gallery wave occurs at a high frequency when the circumference of the scatter is nearly an integer multiple of the wavelength and transports along the circumferential direction at the fluid/solid interface. On the other hand, the resonances here in the PM cloak happen when the shear wave travelling back and forth along the radial direction experiences a phase change by an integer multiply of 2π. This explains why the peaks in each order of scattering coefficient are repeated and almost equally spaced. The peak spacing in each scattering order can be roughly estimated as $\Delta ka/\pi = c_{\mathrm{T}}/c_0$, in which c_{T} is the shear wave speed in cloak material. In the present example, $\Delta ka/\pi \approx \sqrt{\zeta\rho_0/\rho} = 0.0936$, which agrees quite well with Fig. 2b. Another difference of the shear resonance compared with the whispering-gallery wave is that it can occur at very low frequency.

3.2. PM Imperfectness and Inner Boundary Condition

We have shown that expected broadband invisibility is punctured by the resonance scattering peaks caused by the unideal PM. To be instructive for the PM design, it is valuable to know how perfect a PM should be realized to obtain the demanded cloaking.

When the characteristic parameters ξ and η remain unchanged, and ζ is set to a smaller value of 0.001, as shown in Fig. 4a, the shear resonances tend to be extremely narrow and the resonance peaks become much denser. This can be understood as a smaller ζ dictating a smaller $G_{r\theta}$ responsible for the shear mode in the current axisymmetric model as mentioned in the previous subsection. Since the shear wave speed along the radial direction decreases, the peak spacing will decrease. Although there are more peaks within a given band, they are narrow and easy to be eliminated by damping. When ζ is enlarged to 0.1 and the cloak material is far away from the PM, as shown in Fig. 4b, the spacing and width of peaks are enlarged and the broadband concealing deteriorates. When keeping ζ unchanged and varying η or ξ, it is found that the resonance peaks translate along the horizontal axis as a whole, while the peak spacing and width are almost unchanged, as shown in Fig. 4c, d with different values of η. Thus in microstructural design of PM cloak, besides the main parameters (ρ, K_r, $K_\perp$), the imperfectness parameter ζ is more critical for getting expected invisibility within targeted frequency bands. When all the three imperfectness parameters approach the ideal values simultaneously, the resonance peaks will be squeezed and a cloak with ideal PM will be recovered.

Figure 5a, b show the TSCS curve and the corresponding scattering coefficient amplitude of order 0∼3 for free inner boundary. All other parameters are the same as those in the previous subsection. It is found that compared with Fig. 2 for the fixed inner boundary, a very wide peak occurs within the $ka/\pi = 0$ ∼0.5 band which cannot be suppressed by damping, which thereby destroys the broadband invisibility. The wide peak originates from the 0th-order scattering and can be explained as the cavity

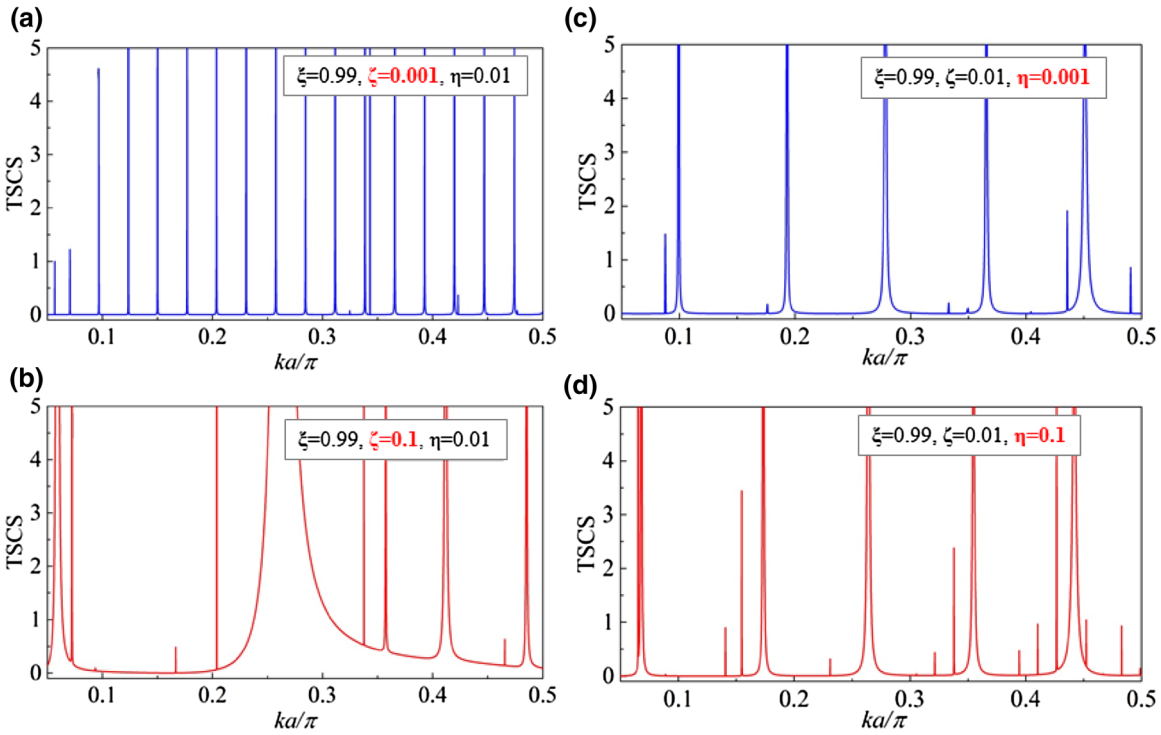

Fig. 4. TSCS spectrum with fixed inner boundary under various imperfectness parameters

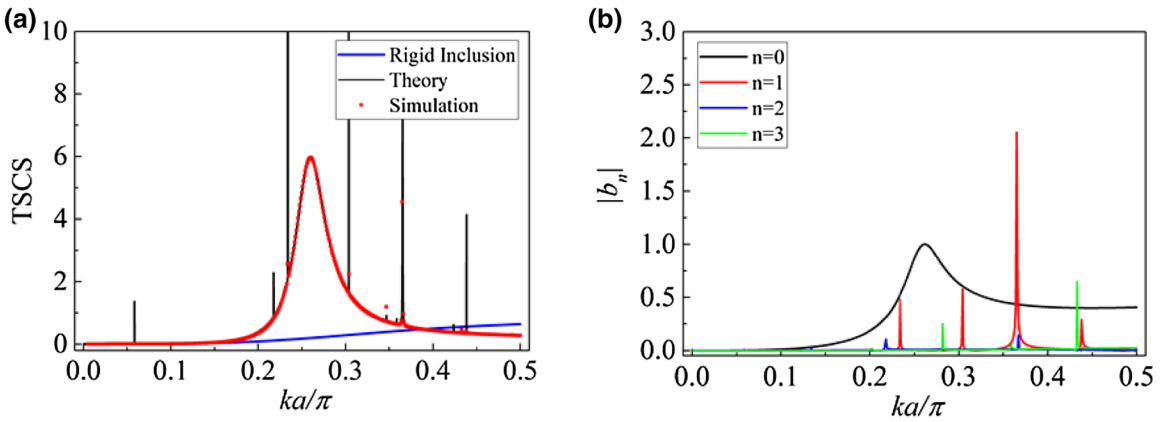

Fig. 5. TSCS spectrum for the case of free inner boundary

resonance, while the narrow ones of higher orders are related to shear resonance. Cavity resonance is attributed to the longitudinal mode, and therefore, is independent of the shear rigidity. Such cavity resonant scattering is also observed in the acoustic cloak with anisotropic density [35].

We have also calculated the scattering spectrum with radially fixed inner boundary. It is revealed that the resulting peaks are further narrower than those of the totally fixed boundary, thus producing the best choice for broadband concealing. However, from the viewpoint of implementation, radially fixed boundary is difficult to apply, while the simplest free inner boundary is not acceptable as shown due to the cavity resonance. To solve this problem, we propose to support the cloak's inner boundary by a homogeneous lining shell. The cloak and shell are perfectly bonded and the inner surface of the shell is left free. By altering the thickness of the lining shell, we can continuously tune the constraint strength on the cloak's inner surface. The proposed scheme not only provides a feasible inner boundary but also offers further insight into the boundary effect of the cloak. For demonstration, steel with density

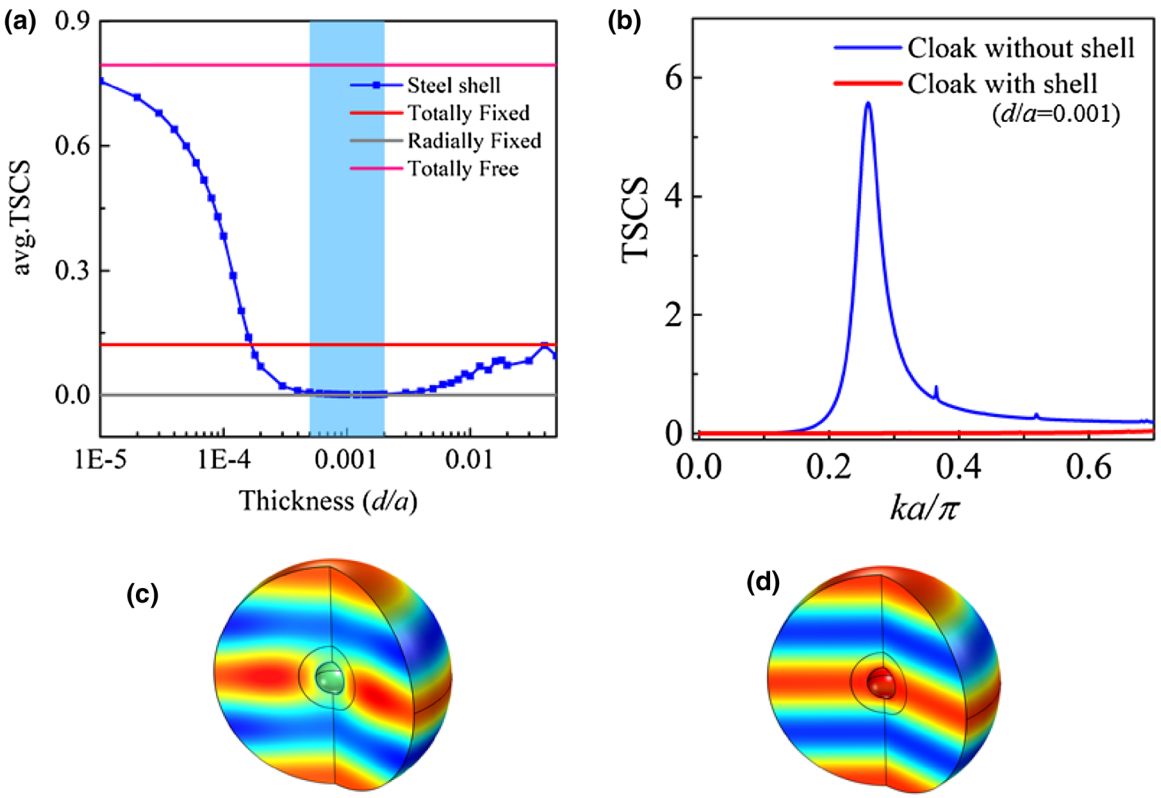

Fig. 6. **a** Averaged TSCS as a function of the thickness of the lining shell; **b** TSCS spectra for cloaks with and without lining shell; pressure fields for cloaks **c** without and **d** with shell, $ka/\pi = 0.3$

$\rho_{\text{steel}} = 7800$ kg/m^3, Young's modulus $E_{\text{steel}} = 220$ GPa and Poisson's ratio $\upsilon_{\text{steel}} = 0.28$ is chosen as the lining shell material.

Figure 6a plots the TSCS as function of the lining shell thickness d normalized by thickness $a$of the cloak. The TSCS is estimated in an average sense over the frequency band $ka/\pi = 0 \sim 0.5$. In order to erase the very narrow resonance peaks, viscous damping of 0.5% is assumed for the PM, i.e. the moduli are multiplied by $1+0.005i$. Average scattering of the three typical inner boundary conditions are marked in the figure as well. As expected, when the cloak is supported by thinner lining shell, the averaged TSCS (the blue curve) is close to the case of free inner boundary. There is an intermediate range of thickness for which the cloak achieves desirable concealing effect for the considered frequency band. In particular, when $d/a = 0.0005 \sim 0.002$, it mimics the radially fixed boundary. Further, increasing the lining thickness will increase the constraint strength and eventually the scattering goes to the result of totally fixed case.

To show the advantage of the lining shell, we plot the TSCS spectra for the cloaks without and with shell (of thickness $d/a = 0.001$) in Fig. 6b. It is seen that for the cloak with lining, the scattering peaks are very thin and are successfully erased with the help of material damping, thus excellent broadband cloaking is achieved. The snapshots of acoustic pressure fields for the two cases at $ka/\pi = 0.3$ are visualized in Fig. 6c, d.

4. Optimization of Layered Cloak Over Targeted Frequency Range

In the forgoing analysis, the cloak material parameters are assumed to be continuously varying. Note that although in the evaluation of scattering, the cloak is discretized in layers, the layer number N is very large to approximate continuous parameters. Actually, to ease the microstructural implementation, it is preferable for the cloak to have several layers with piecewise constant properties, considering the practical limitation of producing smoothly gradient PM unit cells [28]. Theoretically, reduction in a continuous cloak to layered version would degenerate the concealing overall, and the resonance peaks

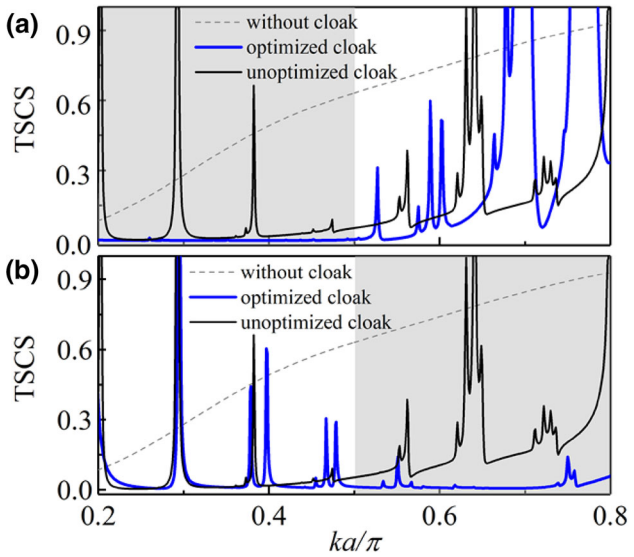

Fig. 7. Optimized TSCS spectra of four-layer cloaks for frequency bands **a** $ka/\pi = 0.2 - 0.5$ and **b** $ka/\pi = 0.5 - 0.8$, respectively

resulting from the unideal PM will complicate the situation. By combining the developed theoretical model with an optimization algorithm, we explore in this section the possibility of achieving effective invisibility within targeted frequency band for unideal PM cloak containing a limited number of layers.

The following optimization procedure is adopted. First, determine the cloak configuration including cloak thickness and inner boundary type, the desired optimization frequency band and the number of layers. Assign initial materials properties $(\rho, K_r, K_\perp)$ by using the transformation method (Eqs. (7)–(9)) in which $-r$ takes the middle location of each layer. Imperfectness parameters are also assigned as well. The developed theoretical approach is naturally suitable for scattering evaluation of layered cloak, it is however noted that sufficient discretization in each constant layer here is still necessary to ensure the accuracy of the state space formulation. The optimization objective function is taken as the average TSCS evaluated by sampling evenly spaced points in the desired frequency band. Then, the built-in MATLAB unconstrained multivariable optimization function *fminsearch* is used to further improve the parameters $(\rho, K_r, K_\perp)$ for each layer under reasonable limitations until convergent result is found.

As a demonstrating example, optimization of a four-layer spherical cloak with inner radius a, outer radius $2a$ and fixed inner boundary is conducted. Imperfectness parameters $\xi = 0.99$, $\zeta = \eta = 0.01$ are assumed. In order to avoid unrealistic optimization results, allowable range of magnitudes and anisotropy of the PM density and moduli must be bounded. In consideration of common PM design technique, parameter variation of each PM layer is constrained by $0.5 < \rho/\rho_0 < 2$, $0.05 < K_r/K_0 < 1$ and $1 < K_\perp/K_0 < 4$. The cloak is evenly divided into four layers with thickness $a/4$. In the optimization process, 100 frequency points per $0.1ka/\pi$ are sampled in the band to evaluate average TSCS, termination error of the objective function optimization variables is 0.001 and the maximum number of iterations is 1000. We assume 0.3% viscous damping in PM material to eliminate the sharp peaks and let the optimization algorithm tackle the unwanted wide ones.

Figure 7a, b show the comparison of TSCS spectra of cloak raw and optimized layer parameters for two different targeted frequency bands $ka/\pi = 0.2 - 0.5$ and $ka/\pi = 0.5 - 0.8$ indicated by grey shades, respectively. It is seen that by breaking the continuous cloak in four constant layers and before the optimization, the concealing effect maintains in low-frequency zone ($ka/\pi < 0.4$) and deteriorates rapidly as the frequency goes up (the black curve), comparing with Fig. 2a. In Fig. 7a, after the optimization, the scattering is almost zero consistently in $ka/\pi = 0.2 - 0.5$ range. In particular, several peaks are removed from the shading area, showing excellent cloaking performance. For the targeted band in high-frequency section, more pronounced gain from the optimization is observed from Fig. 7b since the original TSCS is very high with giant peaks; however, it is hard to get a plainly low TSCS curve

Table 1. **Material parameters in optimization of cloak of thickness a upon targeted frequency bands $ka/\pi = 0.2 - 0.5$ and $ka/\pi = 0.5 - 0.8$**

Layer	Initial			$ka/\pi = 0.2 - 0.5$			$ka/\pi = 0.5 - 0.8$		
	ρ/ρ_0	K_r/K_0	$K_\perp/K_0$	ρ/ρ_0	K_r/K_0	$K_\perp/K_0$	$\rho/\ \rho_0$	K_r/K_0	$K_\perp/K_0$
1	1.1417	0.2123	2.3189	1.0567	0.0991	1.8084	0.8077	0.1487	2.3703
2	1.1417	0.5502	1.4405	0.9930	0.4591	1.9365	0.5000	0.7735	1.2814
3	1.1417	0.7358	1.2456	1.2112	0.8541	1.7699	1.9828	0.3757	1.9165
4	1.1417	0.8407	1.1654	1.2854	0.6953	1.0584	1.1439	0.7402	1.3481

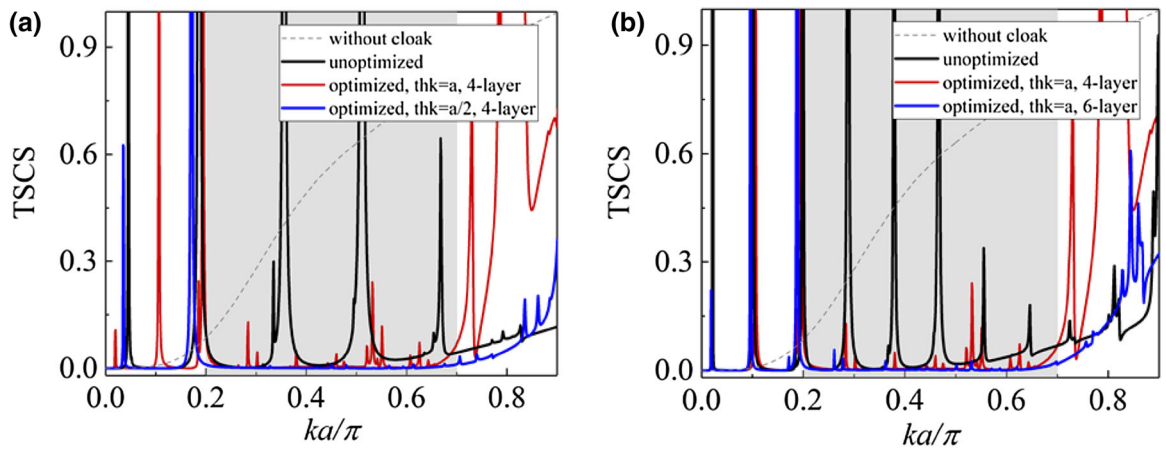

Fig. 8. Optimization results for the cloak **a** with a thinner thickness and **b** with more layers, respectively. (Color figure online)

as in low frequency band. Generally, as the optimization improves the performance in the interested frequency, the cloaking effect will be correspondingly worsened out of that band. Initial and optimized layer parameters are listed in Table 1.

It can be anticipated that if the layer number is fixed, say, for a four-layer cloak, thinner thickness of the cloak will be more preferable owing to not only the smaller overall cloak size but also the better performance resulting from more compact layer stepping. However, meanwhile the required material properties will be more stringent. To show this, we consider again the previous four-layer cloak with the thickness reduced from a to $a/2$, and conduct an optimization under a wider frequency range $ka/\pi = 0.2 - 0.7$. The results are shown in Fig. 8a, where the TSCS spectra before and after optimization are shown by black and blue curves, respectively. The optimized result for case of cloak of thickness a is also shown in the figure in red as well. It is seen that very good broadband invisibility is achieved for the cloak of $a/2$ thickness, and the quite wide resonance peaks in the band are removed by the optimization, while degraded performance is observed for the cloak of larger thickness. The initial and optimized layer parameters are listed in Table 2, showing steeper PM properties compared with Table 1. In this regard, it is advantageous to select thinner thickness for layered cloak whenever possible, as long as the material properties are available from PM design. Of course, better performance should also be obtained by increasing the layer number. Figure 8b displays the optimized result for six-layer cloak with thickness a upon $ka/\pi = 0.2-0.7$ band. With the layer number increased, the shear resonance peaks turn narrower and denser originally, but can be more effectively removed within the wanted band by optimization procedure compare with the four-layer result shown in the figure as well.

5. Conclusion

In this paper, a theoretical formulation for acoustic scattering is developed using the state space approach for spherical cloak composed of unideal PM with small shear rigidity. With the developed method, the general scattering nature and influence of PM imperfectness and inner boundary condition on the cloaking effect are systematically investigated. It is found that the shear rigidity of unideal

Table 2. **Material parameters in optimization of cloak of thickness $a/2$ upon targeted frequency band $ka/\pi = 0.2 - 0.7$**

layer	initial			$ka/\pi = 0.2 - 0.7$		
	ρ/ρ_0	K_r/K_0	$K_\perp/K_0$	ρ/ρ_0	K_r/K_0	$K_\perp/K_0$
1	1.4177	0.1066	3.6464	1.1436	0.0500	3.9985
2	1.4177	0.3379	2.0482	1.1967	0.1728	2.4521
3	1.4177	0.5188	1.6531	1.5737	0.4172	2.5855
4	1.4177	0.6524	1.4741	1.9569	0.5153	1.7793

PM creates standing shear wave mode in cloak material, which results in regularly scattering peaks spreading in full spectrum, and the cloak's broadband effectiveness is damaged. Although the scattering peaks are unavoidable, sharp peaks are in general more preferable because they might hopefully be erased from the spectrum by inherent material damping. In this regard, it is found that the radially fixed inner boundary constraint is better, while the imperfectness parameter ζ is more responsible for getting removable peaks. To overcome the difficulty in realization of the appropriate inner boundary, we propose a lining shell scheme to flexibly tune the constraint strength for best scattering spectrum. Finally, with the help of efficient theoretical model and optimization algorithm, we are able to simplify the continuous cloak to a few piecewise constant layers which will greatly ease its realization, and achieve excellent invisibility in targeted frequency bands. The work is valuable towards further microstructural implementations of 3D spherical PM cloaks.

Acknowledgements. This work was supported in part by the National Natural Science Foundation of China (Grant Nos. 11372035, 11632003, 11472044, 11802017) and the Postdoctoral Innovation Talent Support Program (No. BX20180040).

References

[1] Leonhardt U. Optical conformal mapping. Science. 2006;312:1777–80.
[2] Pendry JB, Schurig D, Smith DR. Controlling electromagnetic fields. Science. 2006;312:1780–2.
[3] Smith DR, Padilla WJ, Vier DC, Nemat-Nasser SC, Schultz S. Composite medium with simultaneously negative permeability and permittivity. Phys Rev Lett. 2000;84:4184–7.
[4] Nassar H, Chen YY, Huang GL. A degenerate polar lattice for cloaking in full two-dimensional elastodynamics and statics. Proc R Soc A. 2019;474:20180523.
[5] Nassar H, Chen YY, Huang GL. Isotropic polar solids for conformal transformation elasticity and cloaking. J Mech Phys Solids. 2019;129:229–43.
[6] Cummer SA, Schurig D. One path to acoustic cloaking. N J Phys. 2007;9:45.
[7] Chen HY, Chan CT. Acoustic cloaking in three dimensions using acoustic metamaterials. Appl Phys Lett. 2007;91:183518.
[8] Christensen J, de Abajo FJG. Anisotropic metamaterials for full control of acoustic waves. Phys Rev Lett. 2012;108:124301.
[9] Milton GW, Willis JR. On modifications of Newton's second law and linear continuum elastodynamics. Proc R Soc A. 2007;463:855–80.
[10] Torrent D, Sanchez-Dehesa J. Anisotropic mass density by radially periodic fluid structures. Phys Rev Lett. 2010;105:430117.
[11] Popa BI, Wang W, Konneker A, Cummer SA, Rohde CA, Martin TP, Orris GJ, Guild MD. Anisotropic acoustic metafluid for underwater operation. J Acoust Soc Am. 2016;139:3325.
[12] Popa B, Zigoneanu L, Cummer SA. Experimental acoustic ground cloak in air. Phys Rev Lett. 2011;106:253901.
[13] Milton GW, Cherkaev AV. Which elasticity tensors are realizable? J Eng Mater Technol. 1995;117:483–93.
[14] Norris AN. Acoustic cloaking theory. Proc R Soc A. 2008;464:2411–34.
[15] Gokhale NH, Cipolla JL, Norris AN. Special transformations for pentamode acoustic cloaking. J Acoust Soc Am. 2012;132:2932–41.
[16] Chen Y, Liu X, Hu G. Design of arbitrary shaped pentamode acoustic cloak based on quasi-symmetric mapping gradient algorithm. J Acoust Soc Am. 2016;140:L405–9.
[17] Cipolla J, Gokhale N, Norris A, Nagy A. Design of inhomogeneous pentamode metamaterials for minimization of scattering. J Acoust Soc Am. 2011;130:2332.
[18] Layman CN, Naify CJ, Martin TP, Calvo DC, Orris GJ. Highly anisotropic elements for acoustic pentamode applications. Phys Rev Lett. 2013;111:24302.
[19] Hladky-Hennion AC, Vasseur JO, Haw G, Croenne C, Haumesser L, Norris AN. Negative refraction of acoustic waves using a foam-like metallic structure. Appl Phys Lett. 2013;102:144103.

[20] Cai X, Wang L, Zhao Z, Zhao A, Zhang X, Wu T, Chen H. The mechanical and acoustic properties of two-dimensional pentamode metamaterials with different structural parameters. Appl Phys Lett. 2016;109:131904.
[21] Zhao A, Zhao Z, Zhang X, Cai X, Wang L, Wu T, Chen H. Design and experimental verification of a water-like pentamode material. Appl Phys Lett. 2017;110:011907.
[22] Zhaoyong S, Han J, Yi C, Zhen W, Jun Y. Design of an underwater acoustic bend by pentamode metafluid. J Acoust Soc Am. 2018;143:1029.
[23] Kadic M, Bückmann T, Stenger N, Thiel M, Wegener M. On the practicability of pentamode mechanical metamaterials. Appl Phys Lett. 2012;100:191901.
[24] Kadic M, Bückmann T, Schittny R, Wegener M. On anisotropic versions of three-dimensional pentamode metamaterials. N J Phys. 2013;15:023029.
[25] Schittny R, Bückmann T, Kadic M, Wegener M. Elastic measurements on macroscopic three-dimensional pentamode metamaterials. Appl Phys Lett. 2013;103:231905.
[26] Huang Y, Lu XG, Liang GY, Xu Z. Pentamodal property and acoustic band gaps of pentamode metamaterials with different cross-section shapes. Phys Lett A. 2016;380:1334–8.
[27] Chen Y, Liu XN, Hu GK. Latticed pentamode acoustic cloak. Sci Rep. 2015;5:15745.
[28] Chen Y, Zheng M, Liu X, Bi Y, Sun Z, Xiang P, Yang J, Hu G. Broadband solid cloak for underwater acoustics. Phys Rev B. 2017;95:180104.
[29] Scandrett CL, Boisvert JE, Howarth TR. Acoustic cloaking using layered pentamode materials. J Acoust Soc Am. 2010;127:2856–64.
[30] Scandrett CL, Boisvert JE, Howarth TR. Broadband optimization of a pentamode-layered spherical acoustic waveguide. Wave Motion. 2011;48:505–14.
[31] Chen WQ, Bian ZG, Ding HJ. Three-dimensional vibration analysis of fluid-filled orthotropic FGM cylindrical shells. Int J Mech Sci. 2004;46:159–71.
[32] Hasheminejad SM, Rajabi M. Acoustic resonance scattering from a submerged functionally graded cylindrical shell. J Sound Vibr. 2007;302:208–28.
[33] Flax L, Dragonette LR, Überall H. Theory of elastic resonance excitation by sound scattering. J Acoust Soc Am. 1978;63:723.
[34] Norris AN. Resonant acoustic scattering from solid targets. J Acoust Soc Am. 1990;88:505.
[35] Cheng Y, Liu XJ. Resonance effects in broadband acoustic cloak with multilayered homogeneous isotropic materials. Appl Phys Lett. 2008;93:71903.

Appendix

The momentum equilibrium, geometric and constitutive equations in cloak's spherical coordinates are listed here,

$$\begin{aligned}
&\frac{\partial\sigma_r}{\partial r}+\frac{1}{r}\frac{\partial\sigma_{r\theta}}{\partial\theta}+\frac{1}{r\sin\theta}\frac{\partial\sigma_{r\varphi}}{\partial\varphi}+\frac{1}{r}(2\sigma_r-\sigma_\theta-\sigma_\varphi+\sigma_{r\theta}\cot\theta)=-\rho\omega^2u_r\\
&\frac{\partial\sigma_{r\theta}}{\partial r}+\frac{1}{r}\frac{\partial\sigma_\theta}{\partial\theta}+\frac{1}{r\sin\theta}\frac{\partial\sigma_{\theta\varphi}}{\partial\varphi}+\frac{1}{r}(3\sigma_{r\theta}+(\sigma_\theta-\sigma_\varphi)\cot\theta)=-\rho\omega^2u_\theta\\
&\frac{\partial\sigma_{r\varphi}}{\partial r}+\frac{1}{r}\frac{\partial\sigma_{\theta\varphi}}{\partial\theta}+\frac{1}{r\sin\theta}\frac{\partial\sigma_\varphi}{\partial\varphi}+\frac{1}{r}(3\sigma_{r\varphi}+2\sigma_{\theta\varphi}\cot\theta)=-\rho\omega^2u_\varphi
\end{aligned}\tag{A1}$$

$$\begin{aligned}
&\varepsilon_\theta=\frac{u_r}{r}+\frac{1}{r}\frac{\partial u_\theta}{\partial\theta},\quad \varepsilon_\varphi=\frac{1}{r\sin\theta}\frac{\partial u_\varphi}{\partial\varphi}+\frac{u_\theta}{r}\cot\theta+\frac{u_r}{r},\quad \gamma_{r\theta}=\frac{1}{r}\frac{\partial u_r}{\partial\theta}+\frac{\partial u_\theta}{\partial r}-\frac{u_\theta}{r}\\
&\gamma_{r\varphi}=\frac{1}{r\sin\theta}\frac{\partial u_r}{\partial\varphi}+\frac{\partial u_\varphi}{\partial r}-\frac{u_\varphi}{r},\quad \gamma_{\theta\varphi}=\frac{1}{r}\left(\frac{\partial u_\varphi}{\partial\theta}-u_\varphi\cot\theta\right)+\frac{1}{r\sin\theta}\frac{\partial u_\theta}{\partial\varphi},\quad \varepsilon_r=\frac{\partial u_r}{\partial r}
\end{aligned}\tag{A2}$$

$$\begin{pmatrix}\sigma_r\\ \sigma_\theta\\ \sigma_\varphi\\ \sigma_{r\theta}\\ \sigma_{r\varphi}\\ \sigma_{\theta\varphi}\end{pmatrix}=K_0\begin{pmatrix}K_r & K_{r\theta} & K_{r\theta} & & & \\ K_{r\theta} & K_\theta & K_\theta-2G_{\theta\varphi} & & 0 & \\ K_{r\theta} & K_\theta-2G_{\theta\varphi} & K_\theta & & & \\ & & & G_{r\theta} & 0 & 0\\ & 0 & & 0 & G_{r\theta} & 0\\ & & & 0 & 0 & G_{\theta\varphi}\end{pmatrix}\begin{pmatrix}\varepsilon_r\\ \varepsilon_\theta\\ \varepsilon_\varphi\\ \gamma_{r\theta}\\ \gamma_{r\varphi}\\ \gamma_{\theta\varphi}\end{pmatrix}\tag{A3}$$

substituting into which the displacement and stress decomposition Eqs. (13) and (14), the r-dependent state vector and Eq. (15) can be concluded.